Date of publication xxxx 00, 0000, date of current version xxxx 00, 0000.

2.5D Inductive Intertwined Frequency Selective Surface for band-pass and high miniaturization applications

JUAN ANDRÉS VÁSQUEZ-PERALVO[1],(Member, IEEE), ROCIO CHUECA LASHERAS[2], JUAN CARLOS MERLANO DUNCAN[1], (Member, IEEE), SHUAI ZHANG [3], (Member, IEEE) , PAVEL PECHAC [4], VÁCLAV KABOUREK, [4], SYMEON CHATZINOTAS, [1], (Fellow Member, IEEE)

[1]Interdisciplinary Centre for Security Reliability and Trust, University of Luxembourg, 1855 Luxembourg City, Luxembourg (e-mail: juan.vasquez, juan.duncan, symeon.chatzinotas, @uni.lu)

[2]Photonics Technologies Group, Aragon Institute for Engineering Research (I3A), University of Zaragoza, Zaragoza, Spain (e-mail: rchueca@unizar.es)

[3]Antenna, Propagation and Millimeterwave Systems (APMS) Section, Aalborg University, 9220 Aalborg, Denmark (e-mail: pechac, kabouvac@fel.cvut.cz)

[4]Department of Electromagnetic Field, Faculty of Electrical Engineering, Czech Technical University in Prague, Praha 6, Czech Republic (e-mail: sz@es.aau.dk)

Corresponding author: JUAN ANDRÉS VÁSQUEZ-PERALVO (e-mail: juan.vasquez@uni.lu).

This work was supported by the Luxembourg National Research Fund (FNR), through the CORE Project (C^3): Cosmic Communications Constructions, under Grant C23/IS/18116142

ABSTRACT This paper presents a detailed design, simulation, measurement, and validation of an Inductive Intertwined Frequency Selective Surface (IIFSS) employing a 2.5D configuration (2.5DIIFSS). The proposed unit cell achieves high miniaturization, with dimensions as small as $0.0096\lambda_0 \times 0.0096\lambda_0$ at 0.268 GHz, using 4 vias per unit cell. The compact design delivers a fractional bandwidth of 87% for the passband associated with the fundamental harmonic. Additionally, the unique 2.5D configuration introduces extra inductance and capacitance, effectively shifting higher harmonics to higher frequencies, thus maintaining a stable stop band beyond the fundamental harmonic. The angular stability analysis reveals minimal variation up to an incidence angle of 60° for both TE and TM modes across the fundamental harmonic. To elucidate the underlying physics, an equivalent circuit model was developed, accurately capturing the fundamental harmonic behavior of the structure. To further validate the design and demonstrate its scalability, a prototype was designed and fabricated for operation at 2.4 GHz, addressing the measurement challenges associated with the original 0.268 GHz design. This prototype was rigorously tested in a transmission regime, with measurement results showing good agreement with simulation data, thereby confirming the efficacy and practicality of the proposed design.

INDEX TERMS Frequency Selective Surfaces, metasurfaces, filters, intertwined structures, miniaturization

I. INTRODUCTION

THIS Frequency Selective Surfaces (FSS) are specialized electromagnetic filters designed to selectively reflect or transmit electromagnetic waves based on frequency. Unlike traditional filters, FSS also account for the incidence angle and polarization of the incoming wave [1]. Typically, FSS structures consist of resonant elements arranged in various lattice configurations, such as rectangular, triangular, or irregular patterns.

The miniaturization of unit cells has become a focal point in FSS research, primarily due to the limitations inherent in conventional FSS designs with one-wavelength periodicity. These limitations include space constraints at low frequencies, frequency shifts at different incidence angles, and the proximity to grating lobe regions [1]. Furthermore, applications such as Electromagnetic Band Gap (Electromagnetic Band-Gap (EBG)) structures, which incorporate FSS resonant elements, demand high levels of miniaturization, particularly in applications like mutual coupling reduction in phased arrays. To address these challenges, various miniaturization techniques have been proposed, including the use of convoluted structures [2], intertwined structures [3], [4], Micro-Electro-Mechanical Systems-based FSS (Miniaturized Element Frequency Selective Surface (MEMFSS)) [5], 2.5D FSS (2.5D Frequency Selective Surface (2.5DFSS)) [6], and designs incorporating lumped elements [7].

One of the significant challenges associated with miniaturization techniques is the generation of higher-order harmonics, which can lead to unintended transmission or reflection windows outside the desired frequency band [8]; therefore, the investigation of techniques that allows to suppress the high harmonics are required.

Considering the use of 2.5DFSS, this technique enables the creation of a highly compact unit cell by extending its struc-

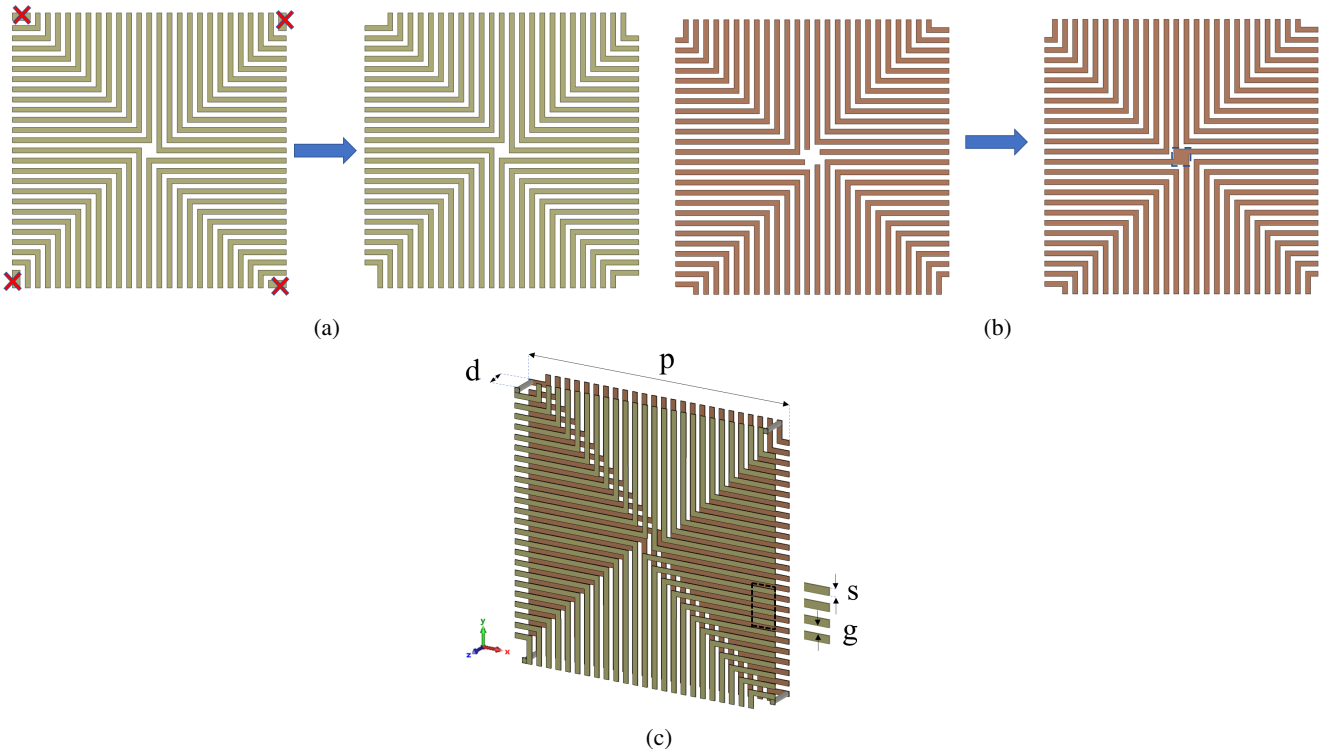

FIGURE 1: 2.5D Inductive Intertwined Frequency Selective Surface (2.5DIIFSS) design phases, corresponding to a fully intertwined unit cell. a) Top layer design. b) Bottom layer design. c) Final unit cell including vias.

ture along the z-axis, as opposed to the conventional x- and y-axis expansion. This miniaturization is achieved through the use of multi-layer FSS interconnected by vias, which lowers the resonance frequency by lengthening the current path across multiple layers. The degree of miniaturization obtained with this approach depends on several factors, including the number of layers, tessellation, substrate thickness, permittivity, and the unit cell's periodicity. In the literature, the application of this technique is generally categorized into two main groups: band-pass and band-stop applications. For band-pass applications, some researchers have proposed the use of knitting structures [9] in combination with FSS geometries such as convoluted structures [10], meandered lines with cavities [11], tapered meandering lines [12], Fibonacci Spiral [13], metal strips, and parallel plates [14]. Others have employed vias to extend the current path instead of using knitting structures, thereby increasing the unit cell length with FSS geometries like hexagonal intertwined designs [3], [15] and convoluted cross-elements [6]. For band-stop applications, the concept of knitting structures has also been utilized, particularly with FSS designs such as meandered capacitive resonators [16], [17] and parallel resonators that produce band-pass characteristics. Some researchers have introduced a secondary inductive resonant structure to generate the pass-band in conjunction with a 2.5DFSS [18]. Additionally, the use of parallel resonator combinations has emerged as another effective strategy for achieving high miniaturization and band-pass characteristics [19]. Other exploratory works investigate the application of four-legged loaded loop structures based on third-order fractal geometries combined with 2.5D structures [20]. The finding of this work is a very compact unit cell allowing a $\frac{\lambda_0}{P} = 29$. Additionally, other researchers have proposed pass-band and stop-band unit cells by employing various layout designs. For instance, the combination of 2.5D structures with convoluted four-fold symmetric designs [21] enables the creation of highly compact structures. Similarly, another study employs capacitance-enhanced, modified Jerusalem cross structures to achieve multiband operation in both transmissive and reflective regimes. This approach is applied to Electromagnetic Interference (EMI) reduction [22]. Both described works have one common drawback, which is the high number of vias required per unit cell.

In the explored literature, 2.5D intertwined, convoluted, and meandered structures have been mainly explored in band stop applications. More over all the previous work uses resonant element that allows to increase the effective electric length of the unit cell (convoluted, intertwined, fractal, knitted, and interwoven), thus resonating to lower frequencies as is the case of the proposed structure. In addition, most of the described research works uses multiple vias which increases the complexity, cost, and leading time of the FSS. However, when it comes to band-pass 2.5D inductive intertwined unit cells, aside from our initial exploratory work presented in [23], there has been no thorough validation of this approach, particularly regarding its capability to suppress higher-order harmonics while providing high miniaturization.

Therefore, this work proposes a 2.5DIIFSS to address the previously identified gap. The proposed unit cell offers sev-

eral key improvements over similar, non-2.5DIIFSS designs found in the literature, including a reduced number of vias, improved miniaturization, and enhanced suppression of high harmonics. This research work most relevant contributions are:

- High miniaturization reaching $\frac{\lambda_0}{P} = 103.378$
- High miniaturization using a relatively low number of vias per unit cell,
- Shifting of high harmonics, overcoming the typical onset of high harmonics at $(2n+1)\lambda_0$,
- Use of intertwined structures applied to bandpass applications being the first work that uses inductive intertwined structures in a 2.5D configuration.

In addition, the key contributions of this manuscript, building upon our previous exploratory work, are as follows:

- Exploration of the performance of the unit cell at higher frequencies,
- Scalability of the unit cell to operate at 2.4 GHz,
- Analysis of the suppression of high-order harmonics,
- Development of an equivalent circuit model that explains the underlying physics and the effect of the configuration on high-order harmonic suppression,
- Manufacturing and measurement of a prototype to validate the initial design and confirm the suppression of high-order harmonics through experimental results.

This paper is organized into six sections. Section II focuses on the design of the unit cell, providing a detailed methodology for developing the 2.5DIIFSS and discussing key design considerations, including the final unit cell dimensions. This section also includes simulation results for the base substrateless unit cell. Section III presents the simulation results for the proposed unit cell, covering the analysis of angular stability, high harmonic suppression, a parametric study, and the development of an equivalent circuit model. In Section IV, our results are compared with similar published works, with adjustments made to the proposed unit cell's dimensions and substrate to ensure a fair and accurate comparison. Section V details the fabrication of the unit cell, scaled for operation at 2.4 GHz, and compares the measurement results with the simulations. Finally, Section VI concludes the paper by summarizing the key findings from the design and measurement phases and suggesting potential directions for future research.

II. UNIT CELL DESIGN

The design concept of this structure follows Babinet's principle applied to the capacitive intertwined structure, that is, obtaining the complementary structure and interconnection of structures. To accomplish this, we take the example of a patch FSS and its complementary, a parch grid FSS, as a starting point. The unit cells in the patch FSS have no electric connection to each of the neighbour unit cells; in other words, they are conductively isolated with each other. On the other hand, the patch grid FSS has electric connections between its neighbouring unit cells at every point where metal is present. Considering the 2.5D Capacitive Inductive Frequency Selective Surface (2.5DCIFSS) presented in [3], the proposed unit cell has no electric connection between neighbor unit cells because its arms are isolated at every point. Therefore, the 2.5DIIFSS design involves obtaining the complementary structure and joining its arms termination by placing a short circuit in the second layer. The design steps that describe the previous statement for designing a 2.5DIIFSS are illustrated in Figure 1 and detailed below.

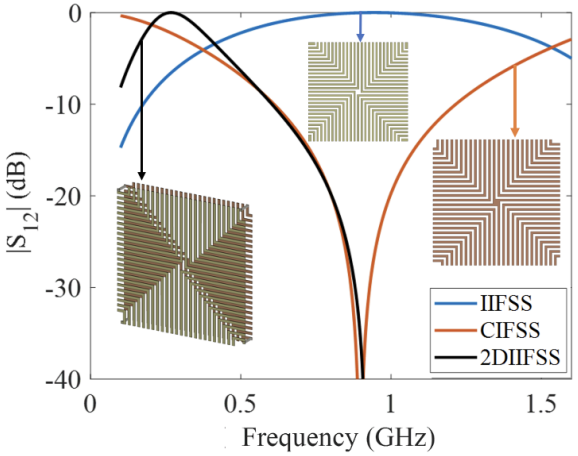

FIGURE 2: $|S_{12}|$ simulation results of the three stages of design of the proposed 2.5DIIFSS, presented in Figure 1

- Design the Inductive Intertwined Frequency Selective Surface (IIFSS) and remove the short circuit at the end of the intertwined arms in the first layer.
- Design the second layer by shifting the arms in the position of the gaps and vice-versa.
- Add a short circuit at the center of the second layer, connecting all the arms.
- Connect the loose arms of the first and second layers using vias.

III. SIMULATION & RESULTS ANALYSIS

In this section we will address the unit cell simulations, an incidence angle analysis, the suppression of high harmonics, parametric studio of the structure, and its equivalent circuit simulation.

1) Unit Cell Simulation

To offer a clearer understanding of the performance of the proposed unit cell, we present the simulation results in Figure 2, corresponding to the three stages of the unit cell design previously shown in Figure 1. These simulations were conducted using CST Microwave Studio, employing the frequency domain solver, which is well-suited for analyzing the high resonance characteristics of the structure.

The unit cell dimensions were carefully selected to align with those used in previously published works [3], [15], [24]. These dimensions are as follows: period $p = 10.8$ mm, arm width $s = 0.2$ mm, inter-arm spacing $g = 0.2$ mm, and substrate thickness $t = 1$ mm. Those unit cell dimensions will allow us to have a fair comparison in terms of minia-

turization. All structures were characterized using the $|S_{12}|$ parameter. As noted in the abstract, to ensure fairness and objectivity in comparison, no dielectric material was used, as its permittivity could cause a shift in the resonance frequency. This choice does not imply that the structure only functions without a substrate, but rather it ensures consistency across comparisons.

In the figure, the IIFSS structure, represented by the blue line, exhibits bandpass behavior with its fundamental harmonic at 0.94 GHz. In contrast, its complementary structure, Capacitive Intertwined Frequency Selective Surface (CIFSS), shown by the orange line, demonstrates band-stop behavior with a fundamental harmonic at 0.898 GHz. Finally, the 2.5DIIFSS, which is derived by interconnecting the previous two structures, is depicted by the black line and shows pass-band behavior with a fundamental harmonic at 0.2687 GHz. The results indicate that by utilizing the 2.5D configuration, the fundamental harmonic has been significantly downward shifted, resulting in a frequency nearly 3.5 times lower compared to the fundamental harmonic of either IIFSS or CIFSS.

2) Angle of Incidence Analysis

A further analysis to understand the incidence angle stability of the proposed 2.5DIIFSS has been carried on. For this, we have obtained the S-Parameters in the TE- and TM-Mode at four angles of incidence $\theta = 0°, 20°, 40°$ and $60°$, and presented in Figure 3. In the analysis we can highlight that independently of the incidence angle, the resonance frequency remains fixed for both modes, at $f_{r_0}^{S_{12},TE} = f_{r_0}^{S_{12},TM} = 0.2687$ GHz for all incident angles. Next, The fractional bandwidth at normal incidence, measured @-3dB, is around $FBW_0^{S_{12},TE} = FBW_0^{S_{12},TM} = 87\%$ GHz for both modes, but it will increase or decrease as the angle of incidence increases for TE-mode and TM-mode, respectively. This variation generally does not depend on ultra-miniaturized unit cells but will rely mainly on the change of the wave impedance, which is a function of the incidence angle. Therefore, this structure is a good candidate for applications where stability under angle of incidence is required for TE- and TM-Mode.

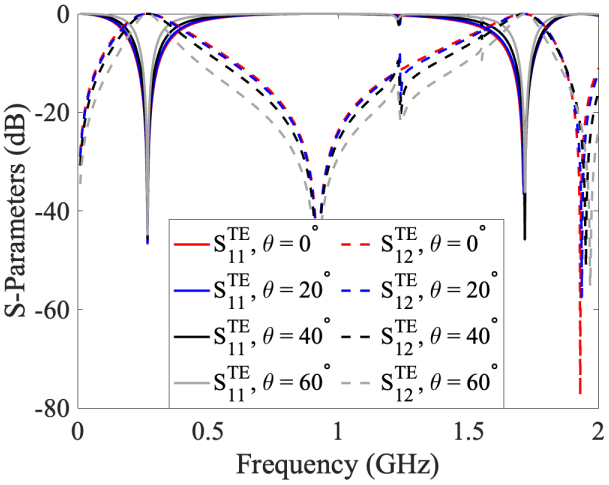

(a)

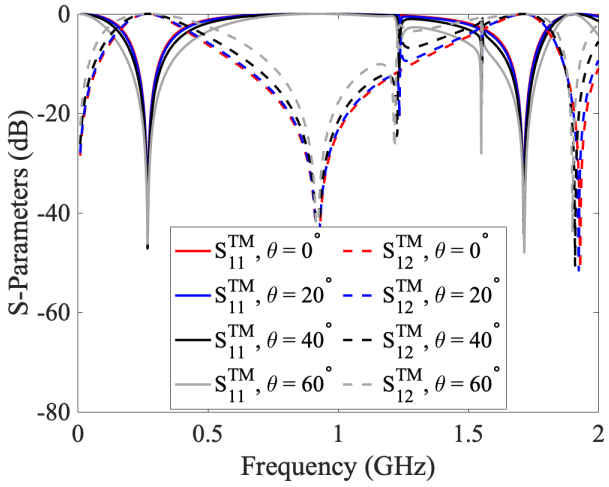

(b)

FIGURE 3: Proposed 2.5DIIFSS S_{11} and S_{12} simulation results at different angles of incidence. Solid lines represent the $S_{11}Hig$ parameter while dashed lines represent the S_{12} parameter. a)TE-Mode, b)TM-Mode.

3) High Harmonic Suppression

In the band-stop region, several noteworthy observations can be made. The proposed 2.5DIIFSS structure exhibits a broad region free of high harmonics compared to a single-layer IIFSS. Intertwined structures essentially consist of folded dipoles intertwined with neighboring dipoles in different lattices, causing high harmonics to appear at odd multiples of $\lambda_0/2$, specifically at $(2n+1)\lambda_0$, where n represents the harmonic number. To show the harmonic-free region of the proposed unit cell, we have designed an IIFSS to resonate at the same fundamental harmonic . This unit cell has a period p_{IIFSS_1} =20.52 mm and the number of intertwined stages to create a complete structure. The results of the proposed unit cell, 2.5DIIFSS, and the scaled, IIFSS, are illustrated in Figure 4.

As observed, the IIFSS exhibits its 3rd and 5th harmonics within the band-stop regions of the proposed 2.5DIIFSS, while the latter has its 3rd harmonic at $6.4\lambda_0$. To better understand this high-order harmonic supresion, it is important to acknowledge that higher-order harmonics are directly related to the physical dimensions and layout of the elements within the unit cell. This implies that any increase or decrease in the unit cell dimensions will cause the higher harmonics to shift in correspondence with the fundamental frequency [8]. Now, to effectively shift the high-order harmonics, we have decreased the unit cell dimensions. The proposed unit cell, 2.5DIIFSS, has a period of $p_{\text{2.5DIIFSS}} = 10.8$ mm, which ensures the shift of the high-order harmonics. However, the fundamental harmonic frequency must remain fixed. For this reason, the use of the 2.5D configuration compensates for the changes in the equivalent capacitance and inductance caused

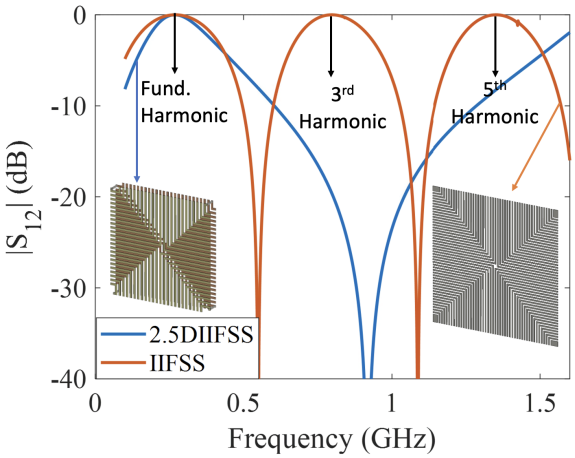

FIGURE 4: $|S_{12}|$ simulation results of the proposed 2.5DIIFSS and the equivalent IIFSS structure to resonate at the same frequency.

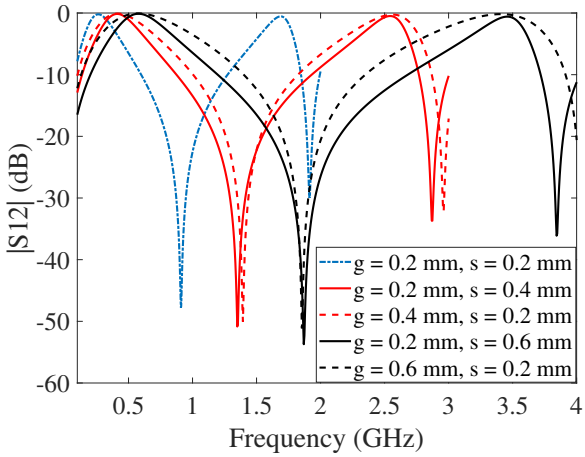

FIGURE 5: 2.5DIIFSS parametric analysis considering the variation of the arm width s and gap between arms g. Results are presented only for TE-mode due to symmetry.

by the reduced unit cell size.

Mathematically, the fundamental harmonic is inversely proportional to the square root of the product of the equivalent inductance and capacitance. Reducing the unit cell dimensions results in a decrease in both the equivalent capacitance and inductance. To counteract this, the 2.5D configuration, along with the capacitive structure at the back, increases the equivalent capacitance and inductance.

The inductance is increased by the extended current path, which effectively lengthens the intertwined arms. The equivalent capacitance is enhanced by the increased surface area available for charge distribution and the parallel plate effect created between the intertwined arms.

4) Parametric Study

The frequency response of the unit cell is closely tied to its dimensions, not only the period but also the width of the intertwined arms and the gap between them (s, g). To explore this relationship, we conducted a parametric study on the effects of varying these parameters, as shown in Figure 5. The figure illustrates five scenarios. The first scenario represents the original configuration with $s = 0.2$ mm and $g = 0.2$ mm, as previously described in the first subsection. In the second and third scenarios (represented by red lines), s is increased to 0.4 mm while keeping $g = 0.2$ mm, and g is increased to 0.4 mm while keeping $s = 0.2$ mm, respectively. The results indicate that in both cases, the frequency response shifts to a higher frequency due to the reduction in the electrical length (less number of intertwined stages) of the unit cell. Although both scenarios exhibit the same frequency shift, the bandwidth differs in each case. For the scenario with a larger gap (g), the equivalent capacitance decreases because the electric field weakens, reducing the structure's ability to store charge which results in low quality factor deriving in a wider bandwidth. Conversely, in the scenario with a wider arm width (s), the inductance decreases because the current has a broader path to traverse, leading to a reduced magnetic field concentration. This reduction in inductance affects the quality factor by increasing it, leading to a narrow bandwidth. In the fourth and fifth scenarios, similar trends are observed, with both frequency responses shifting to higher frequencies due to the increased values of g and s, respectively.

A. UNIT CELL EQUIVALENT CIRCUIT

To gain a deeper understanding of the physics behind the proposed unit cell, we have developed an equivalent circuit model that captures its behavior. Fundamentally, any FSS can be modeled with an equivalent admittance, comprising elements such as resistance, capacitance, inductance, and transmission lines. In this model, the equivalent resistance accounts for the ohmic losses in the copper and the substrate. Due to the nature of this unit cell, which is basically folded dipoles creating mutual inductance and interdigital capacitance, the equivalent circuit is quite straightforward to analyze. The copper traces, along with the gaps between them, represent the equivalent inductances and capacitances, reflecting the geometric distribution of the resonant elements. Finally, the transmission lines in the model correspond to the substrates that separate each of the FSS layers.

The equivalent circuit of the proposed 2.5DIIFSS, illustrated in Figure 6, consists of a shunt circuit ($C_A||L_A$) in series with L_B. In this model, the capacitance C_A represents the equivalent capacitance of the intertwined lines, L_A corresponds to the equivalent inductance of the intertwined lines, and L_B represents the additional inductance introduced by the 2.5D configuration. To determine the numerical values of the equivalent circuit C_A, L_A, and L_B we can relate the equivalent admittance with the simulated S parameters using Eq.1.

$$Y_{\text{eq}} = \Im\left\{\frac{2S_{11}}{\eta_0 S_{12}}\right\} \tag{1}$$

Here, S_{11} denotes the reflection coefficient, S_{12} represents the transmission coefficient, and η_0 is the free-space impedance.

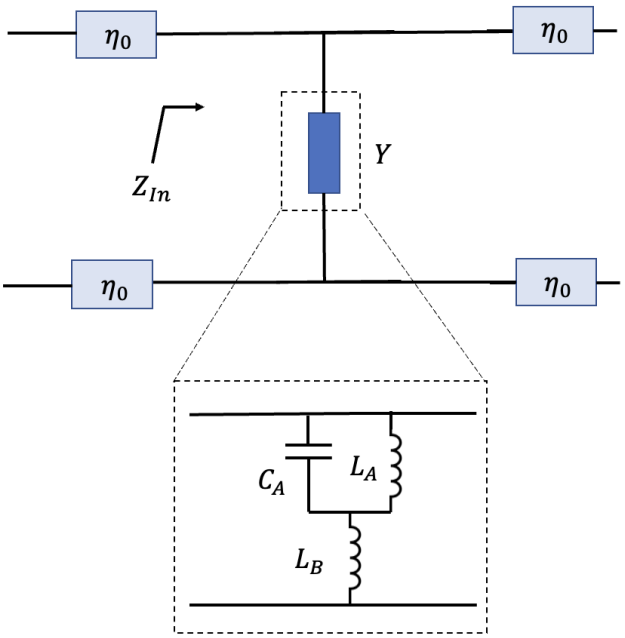

FIGURE 6: Graphical representation of the proposed equivalent circuit for the 2.5DIIFSS

Additionally, the equivalent admittance of the proposed circuit can be derived by solving the equivalent circuit shown in Figure 6, as defined by Eq. (2). It is noteworthy to consider that the effect of the permittivity and thickness of the substrate will be embedded on on the values of the equivalent capacitance and inductance.

$$Y_{\text{eq}} = \left(\frac{\frac{L_A+L_B}{C_A} - \omega^2 L_A L_B}{j\omega L_A + \frac{1}{j\omega C_A}} \right)^{-1} \tag{2}$$

Therefore, the values of C_A, L_A, and L_B can be determined by solving the circuit equations using a preferred iterative method. The calculated values for the circuit elements are: $C_A = 2.8104$ pF, $L_A = 110.3$ nH, and $L_B = 11.7$ nH. The resulting calculated $|S_{12}|$ from the equivalent circuit model is compared against the simulated results, as shown in Figure 7. The comparison demonstrates good agreement, including the presence of a null where the structure functions as a bandstop filter, thereby validating the proposed approach.

IV. COMPARISON WITH SIMILAR PUBLISHED WORK

Finally, to compare the results obtained with the described unit cell against others found in the literature, we have simulated our unit cell to match the same p, t, ϵ_r, s, and g of previous works. Due to the short branch of related works that use 2.5DIIFSS, some comparisons are with either non-2.5D, non-intertwined, or capacitive FSS. Table 1 provides a comprehensive comparison, highlighting several key findings. First, the miniaturization of the unit cell, as indicated by the figure of merit (Figure of Merit (FOM)) $\frac{\lambda_0}{p}$, is significantly higher in the proposed design compared to other works. While this high degree of miniaturization does come with a

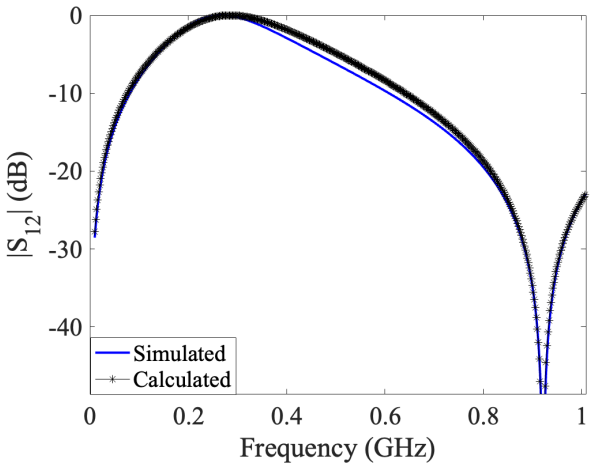

FIGURE 7: Comparison of the computed $|S_{12}|$ using the equivalent circuit method against the simulated.

trade-off in terms of a reduced Fractional Bandwidth (FBW) relative to some counterparts, the proposed design offers other advantages. Notably, the number of pins used in this design is relatively low compared to other 2.5D technologies, which simplifies the design and reduces the time required for pin verification. Additionally, although the number of layers in the proposed unit cell is comparable to those in other studies, it achieves superior miniaturization. Finally, it's worth noting that the compared works primarily focus on the fundamental harmonic and do not analyze the onset of higher harmonics, which presents an opportunity for further research in this area.

V. MANUFACTURING AND MEASUREMENTS

The proposed approach has been validated by manufacturing a scaled version of the analyzed unit cell. The scaling of the unit cell, which means that using the same unit cell design, where increasing or decreasing the size of its elements enables a shift in operating frequency—either lowering or raising it accordingly. This decision was driven by measurement constraints and the need to test the scalability of the design. The measurement constraints stem from the challenges associated with characterizing a structure that resonates at 0.2687 GHz, which would require a setup with very large dimensions. Scaling the design provided an opportunity to assess the structure's scalability by targeting a frequency of interest for practical applications, such as WiFi. Consequently, the structure was redesigned to create a bandpass filter at 2.4 GHz. To validate the design, a prototype was manufactured and tested, with the results compared to the simulations. The prototype, shown in Figure 8, measures 400×400 mm^2 and is printed on a two-sided 0.8 mm thick Rogers 4003C substrate with $\epsilon_r = 3.38$ and $\tan(\delta) = 0.0027$ at 10 GHz. The prototype consists of 5041 unit cells (71x71), with a unit cell period of $p = 2.55$ mm, a gap of $g = 0.15$ mm, and an arm width of $s = 0.15$ mm.

The manufactured prototype is measured using a test bed,

TABLE 1: Comparison of reported unit cells with the current work (CW). (*: FBW at -3dB, +: FBW at -10 dB)

Parameter	Cited Works									
	[18]	[19]	[25]	[26]	[27]	[28]	[3]	[20]	[21]	[22]
p (mm)	2.87	7.8	6	4.3	4.4	7	10.8	9.75	12	8.9
s (mm)	0.2	0.1	0.2	0.2	0.2	0.2	0.2	0.25	0.5	0.25
g (mm)	0.2	0.1	0.2	0.2	0.2	0.2	0.2	0.25	0.5	0.25
t (mm)	0.38	0.254	0.5	0.5	1	0.254	0.6	1.6	1.6	0.8
ϵ_r	2.2	2.2	3	3.55	2.65	4.3	1	4.3	4.3	4.3
$\frac{\lambda_0}{p}$ (Cited)	6.13	16.02	20.66	28.57	17.24	29.41	34.75	29.14	22.72	14.28
Miniat. (λ_0) (Cited)	0.1631	0.0624	0.0484	0.035	0.058	0.034	0.0288	0.0343	0.044	0.07
$\frac{\lambda_0}{p}$ (CW)	26.416	169.75	67	52.45	56.35	72.296	103.648	109.5	65	100.08
Miniat. (λ_0) (CW)	0.0379	0.0059	0.0149	0.0191	0.0177	0.0138	0.0096	0.0091	0.0154	0.01
FBW % (Cited)	<10*	110.2*	49.5*	36.36*	92.5*	21*	92.45^+	9.45^+	18.8^+	17.2^+
FBW % (CW)	62.1*	62.10*	65.6*	64.73*	73.14*	60.64*	33.2^+	23.13^+	22.34^+	21.32^+
Vias (Cited)	24	4	0	0	0	0	6	8	8	8
Vias (CW)	4	4	4	4	4	4	4	4	4	4

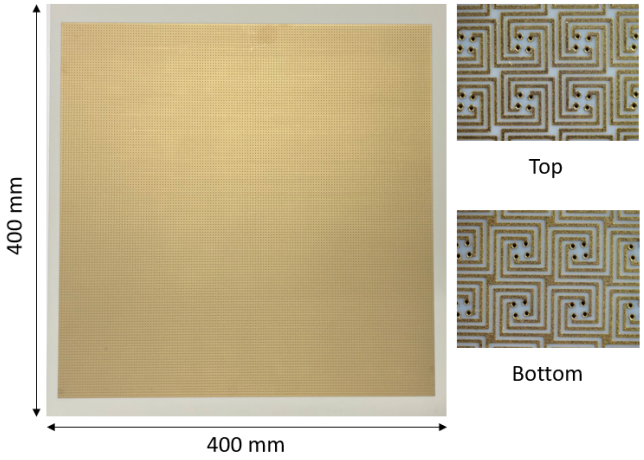

FIGURE 8: Actual photo of the manufactured prototype showing the overall dimensions and top and bottom faces.

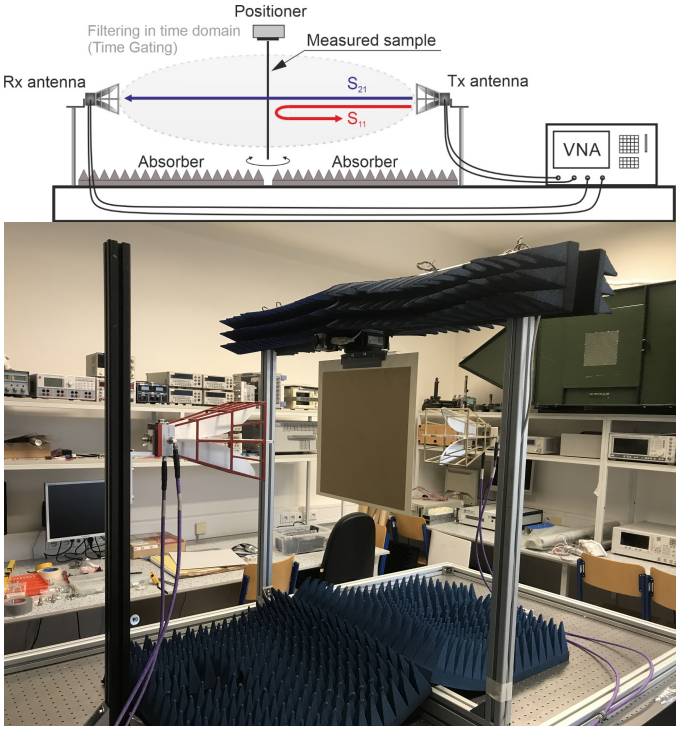

FIGURE 9: Measurement setup showing one of the setup configurations and in normal incidence.

visually depicted in form of a sketch and and actual photo in Figure 9. Prototype is attached to a stepper motor rotator located between transmit and receive dual-polarized quad-ridged horn antennas. Both antennas are connected to a 4-port vector network analyzer Rohde@Schwarz ZVA67 and transmission coefficients S_{xy} are measured simultaneously for both polarizations (TE and TM modes). The illumination angle is set for each measurement by rotating the manufactured prototype in 4 different angles 0°, 20°, 40° and 60°.
All the data are measured in the same frequency bandwidth (100 MHz to 26 GHz). To cover this frequency span, three sets of antennas are used:

- Setup 1: QRH11 antennas and a distance of 656 mm between each antenna to the sample.
- Setup 2: QRH20 antennas and a distance of 872 mm between each antenna to the sample.
- Setup 3: QRH40 antennas and a distance of 1000 mm between each antenna to the sample.

Since the antennas are attached to the fixed stands, distances between them (aperture to aperture) changes. The relatively small size of the fabricated sample in terms of wavelengths causes the diffraction at its edges. The resulting signals, together with multipath signals arising from reflections from surrounding objects, affect the S_{xy} data obtained. Therefore, the time gating is applied to the measured results to extract only the direct transmission through the sample. The measured results have been compared with the corresponding simulated ones

The measured results have been compared with the corresponding simulated results for TE and TM modes at all angles of incidence and are visually presented in Figure 10. The measurements cover a frequency range from 1 GHz to 20 GHz.

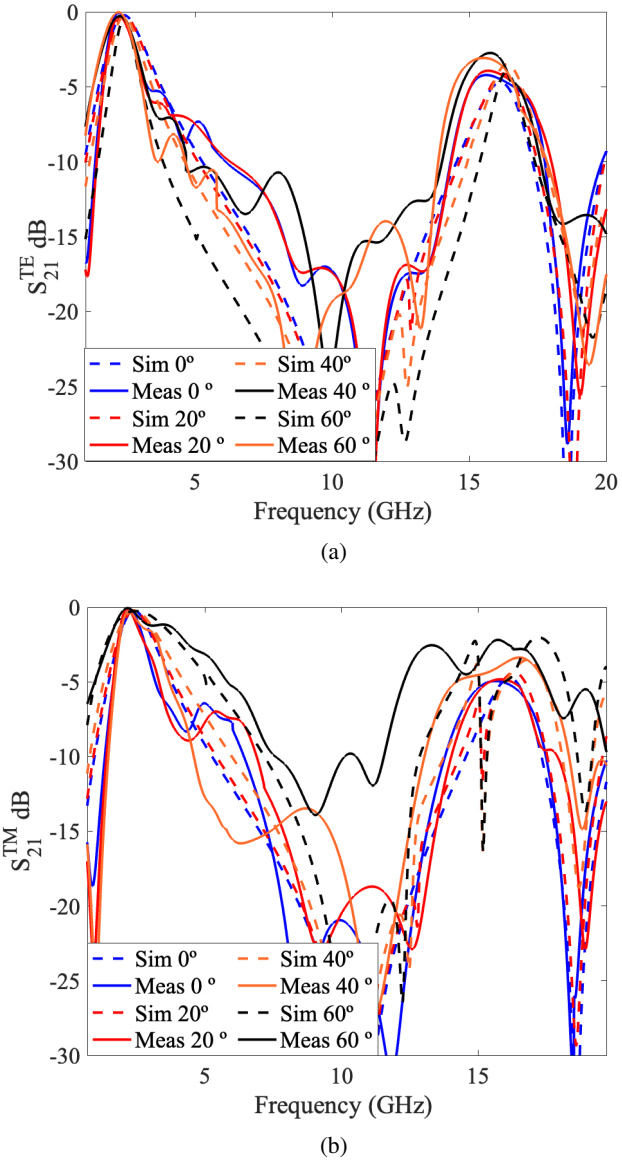

FIGURE 10: Comparison between measured and simulated results. (a) TE mode. (b) TM mode.

For the TE-mode $|S_{12}|$ results, the measured data closely align with the simulations, with the following observations:

- The measured structure fundamental harmonic has been shifted from the desired 2.4 GHz to 2.19 GHz, taking as a reference the results at normal incidence. This shift is mainly attributed to the manufacturing tolerances, specifically to the thickness of the intertwined lines that are thicker than expected. This thickness increases the equivalent capacitance, which reduces the resonant frequency.
- The bandwidth pass has been reduced from 1.61 GHz in simulation to 1.15 GHz in measurements @-3dB in normal incidence. This reduction in bandwidth can also be explained due to tolerances, because this increase in capacitance modifies the quality factor by increasing it deriving in a low bandwidth.
- The angular stability is clearly visible even for high angles of incidence.

For the TM-mode $|S_{12}|$, the correlation between measured and simulated results decreases. In some more elaborated analysis is following presented:

- The angular stability of the structure decreases as the incidence angle increases, particularly at 60°. This variation is primarily caused by the orientation of the electric field relative to the antenna's rotation at different incidence angles. In TE-mode, the E-field is parallel to the rotation axis, minimizing the impact of the structure's proximity to the antenna, even at high incidence angles. However, in TM-mode, the structure's proximity to the horn antenna at high angles results in distortion of the frequency response. To mitigate this effect, lenses or larger Frequency Selective Surface (FSS) structures can be used to increase the separation between the FSS and the horn antenna while maintaining proper illumination.
- The resonance frequency also shifts in TM-mode, with a reduction in bandwidth at normal incidence. However, as the angle of incidence increases, the bandwidth widens due to changes in wave impedance, as discussed in the simulation section.

Finally, the results from both TE and TM modes demonstrate that the structure effectively suppresses high harmonics, preventing their onset within a range of $6.8\lambda_0$ in simulations and $7.1\lambda_0$ in the manufactured prototype at normal incidence. However, in TM mode, this suppression band narrows at different angles of incidence due to changes in wave impedance.

VI. CONCLUSIONS

The proposed unit cell can achieve sub-wavelength miniaturization due to the increased equivalent capacitance and inductance produced by the intertwined and tesselation geometry. Furthermore, the miniaturization can be further improved by the 2.5D configuration that extends the current distribution along both layers. In addition, the angular stability of this unit cell has been proven to work as expected, which can be tested to higher angles of incidence without losing the first band-pass characteristics. One of the key characterisitics of this structure is its wide suppresion band of high harmonics, which has overcome the rule of $(2n+1)\lambda_0$ for the high harmonics onset to approximately values bigger than $6\lambda_0$. The validity of the presented design has been tested by manufacturing and measuring a prototype designed to generate a main pass-band at 2.4 GHz. Finally, the 2.5DIIFSS can be extended to other geometries like the triangular, hexagonal, or circular lattices that can further improve miniaturization, FBW and high harmonic suppresion band.

REFERENCES

[1] B. A. Munk, *Frequency selective surfaces: theory and design*. John Wiley & Sons, 2005.

[2] E. A. Parker, A. d. C. Lima *et al.*, "Convoluted frequency-selective array elements derived from linear and crossed dipoles," in *IEE Proceedings H (Microwaves, Antennas and Propagation)*, vol. 140, no. 5. IET, 1993, pp. 378–380.

[3] J. A. Vásquez-Peralvo, J. M. Fernández-González, J. M. Rigelsford, and P. Valtr, "Interwoven hexagonal frequency selective surface: An application for wifi propagation control," *IEEE Access*, vol. 9, pp. 111 552–111 566, 2021.

[4] J. A. Vásquez-Peralvo, J. M. Fernández-González, and J. M. Rigelsford, "Radar cross section reduction using intertwined structures," in *2021 15th European Conference on Antennas and Propagation (EuCAP)*. IEEE, 2021, pp. 1–5.

[5] K. Sarabandi and N. Behdad, "A frequency selective surface with miniaturized elements," *IEEE Transactions on Antennas and propagation*, vol. 55, no. 5, pp. 1239–1245, 2007.

[6] W. Yin, H. Zhang, T. Zhong, and X. Min, "Ultra-miniaturized low-profile angularly-stable frequency selective surface design," *IEEE Transactions on Electromagnetic Compatibility*, vol. 61, no. 4, pp. 1234–1238, 2019.

[7] N. Liu, X. Sheng, C. Zhang, J. Fan, and D. Guo, "A design method for synthesizing miniaturized fss using lumped reactive components," *IEEE transactions on electromagnetic compatibility*, vol. 60, no. 2, pp. 536–539, 2017.

[8] S. M. A. Momeni Hasan Abadi, M. Li, and N. Behdad, "Harmonic-suppressed miniaturized-element frequency selective surfaces with higher order bandpass responses," *IEEE Transactions on Antennas and Propagation*, vol. 62, no. 5, pp. 2562–2571, 2014.

[9] T. Hussain, Q. Cao, J. K. Kayani, and I. Majid, "Miniaturization of frequency selective surfaces using 2.5-d knitted structures: Design and synthesis," *IEEE Transactions on Antennas and Propagation*, vol. 65, no. 5, pp. 2405–2412, 2017.

[10] M. W. Niaz, Y. Yin, S. Zheng, L. Zhao, and J. Chen, "Design and analysis of an ultraminiaturized fss using 2.5-d convoluted square spirals," *IEEE Transactions on Antennas and Propagation*, vol. 68, no. 4, pp. 2919–2925, 2020.

[11] P.-S. Wei, C.-N. Chiu, and T.-L. Wu, "Design and analysis of an ultra-miniaturized frequency selective surface with two arbitrary stopbands," *IEEE Transactions on Electromagnetic Compatibility*, vol. 61, no. 5, pp. 1447–1456, 2019.

[12] M. W. Niaz, Y. Yin, and J. Chen, "Synthesis of ultraminiaturized frequency-selective surfaces utilizing 2.5-d tapered meandering lines," *IEEE Antennas and Wireless Propagation Letters*, vol. 19, no. 1, pp. 163–167, 2020.

[13] K. K. Varikuntla and R. Singaravelu, "Design of a novel 2.5d frequency selective surface element using fibonacci spiral for radome application," in *2018 Asia-Pacific Microwave Conference (APMC)*, 2018, pp. 1289–1291.

[14] H. Li, F. Costa, J. Fang, L. Liu, Y. Wang, Q. Cao, and A. Monorchio, "2.5-d miniaturized multifunctional active frequency-selective surface," *IEEE Transactions on Antennas and Propagation*, vol. 67, no. 7, pp. 4659–4667, 2019.

[15] J. A. Vásquez-Peralvo, J. C. M. Duncán, J. M. Fernández-González, and S. Chatzinotas, "Triangular intertwined frequency selective surface," in *2022 International Symposium on Antennas and Propagation (ISAP)*, 2022, pp. 35–36.

[16] Z. Yang, W. Jiang, Q. Huang, and T. Hong, "A 2.5-d miniaturized frequency-selective rasorber with a wide high-transmission passband," *IEEE Antennas and Wireless Propagation Letters*, vol. 20, no. 7, pp. 1140–1144, 2021.

[17] Q. Yu, S. Liu, A. Monorchio, X. Kong, D. Brizi, X. Zhang, and L. Wang, "Miniaturized wide-angle rasorber with a wide interabsorption high transparent bandpass based on multiple 2.5-d resonators," *IEEE Antennas and Wireless Propagation Letters*, vol. 21, no. 2, pp. 416–420, 2022.

[18] D. Li, T.-W. Li, E.-P. Li, and Y.-J. Zhang, "A 2.5-d angularly stable frequency selective surface using via-based structure for 5g emi shielding," *IEEE Transactions on Electromagnetic Compatibility*, vol. 60, no. 3, pp. 768–775, 2018.

[19] Y. Ma, W. Wu, Y. Yuan, X. Zhang, and N. Yuan, "A wideband fss based on vias for communication systems," *IEEE Antennas and Wireless Propagation Letters*, vol. 17, no. 12, pp. 2517–2520, 2018.

[20] L. Murugasamy and R. Sivasamy, "A novel fractal inspired iterated four-legged loaded loop elements based 2.5-d miniaturized frequency selective surface," *IEEE Transactions on Electromagnetic Compatibility*, vol. 63, no. 6, pp. 2164–2167, 2021.

[21] S. Ghosh, "A 2.5-dimensional miniaturized frequency selective surface based on convoluted geometry," in *2022 3rd URSI Atlantic and Asia Pacific Radio Science Meeting (AT-AP-RASC)*, 2022, pp. 1–4.

[22] S. Dey and S. Dey, "Miniaturized near all-angle stable 2.5-d fss for dual-band shielding in transmission mode and multiband absorption in reflection mode," *IEEE Transactions on Antennas and Propagation*, vol. 71, no. 9, pp. 7323–7332, 2023.

[23] J. A. Vásquez-Peralvo, J. C. M. Duncán, J. L. González-Rios, and S. Chatzinotas, "2.5 d inductive intertwined frequency selective surface for pass-band applications," in *2023 International Workshop on Antenna Technology (iWAT)*. IEEE, 2023, pp. 1–3.

[24] A. Vallecchi, R. J. Langley, and A. G. Schuchinsky, "Bistate frequency selective surfaces made of intertwined slot arrays," *IEEE Transactions on Antennas and Propagation*, vol. 65, no. 6, pp. 3093–3101, 2017.

[25] P.-C. Zhao, Z.-Y. Zong, W. Wu, and D.-G. Fang, "A convoluted structure for miniaturized frequency selective surface and its equivalent circuit for optimization design," *IEEE Transactions on Antennas and Propagation*, vol. 64, no. 7, pp. 2963–2970, 2016.

[26] P.-C. Zhao, Z.-Y. Zong, W. Wu, B. Li, and D.-G. Fang, "Miniaturized-element bandpass fss by loading capacitive structures," *IEEE Transactions on Antennas and Propagation*, vol. 67, no. 5, pp. 3539–3544, 2019.

[27] M. Yan, S. Qu, J. Wang, J. Zhang, A. Zhang, S. Xia, and W. Wang, "A novel miniaturized frequency selective surface with stable resonance," *IEEE Antennas and Wireless Propagation Letters*, vol. 13, pp. 639–641, 2014.

[28] H. Li, C. Yang, Q. Cao, and Y. Wang, "An ultrathin bandpass frequency selective surface with miniaturized element," *IEEE Antennas and Wireless Propagation Letters*, vol. 16, pp. 341–344, 2016.

JUAN A. VÁSQUEZ-PERALVO (Member IEEE) was born in Quito, Ecuador. He earned his Bachelor of Engineering in Electronics and Telecommunications from Escuela Politécnica Nacional, Quito, Ecuador. He received his Master of Science in Wireless Communication Systems from the University of Sheffield, Sheffield, UK. During his doctoral studies, Juan was a research visitor at the Illinois Institute of Technology (IIT) in Chicago, USA, supervised by Prof. Thomas Wong. In 2022, Juan obtained his Ph.D. in Communication Systems from Universidad Politécnica de Madrid, Madrid, Spain. Currently, Juan is a research scientist at the Université du Luxembourg, specializing in antenna design for satellite communications. His research interests include phased array systems, digital beamforming, additive manufacturing for onboard antennas and user terminals, meta-surfaces, vehicle antennas, and lens antenna design.

ROCIO CHUECA obtained her B. Sc. in Telecommunications and her M. Sc. in Telecommunications Engineering from University of Zaragoza, Zaragoza, Spain, in 2017 and 2019, respectively. She joined he Photonics Technologies Group, Aragon Institute for Engineering Research (I3A), University of Zaragoza as a Researcher in 2017 and work for several projects related to optics, electronics, solar energy and radiofrequency.She started as a PhD student with the Photonics Technologies Group in 2020. Her current research is focus on radiofrequency transmission through energy saving windows that includes frequency selective surfaces, electromagtenic simulations, periodic structures and RF measurements.

JUAN CARLOS MERLANO DUNCAN (S'09-M'12-SM'20) received the Diploma degree in electrical engineering from the Universidad del Norte, Barranquilla, Colombia, in 2004, the M.Sc. and Ph.D. Diploma (Cum Laude) degrees from the Universitat Politècnica de Catalunya (UPC), Barcelona, Spain, in 2009 and 2012, respectively. His research interests are wireless communications, remote sensing, distributed systems, frequency distribution and carrier synchronization systems, software-defined radios, and embedded systems. At UPC, he was responsible for the design and implementation of a radar system known as SABRINA, which was the first ground-based bistatic radar receiver using space-borne platforms, such as ERS-2, ENVISAT, and TerraSAR-X as opportunity transmitters (C and X bands). He was also in charge of the implementation of a ground-based array of transmitters, which was able to monitor land subsidence with subwavelength precision. These two implementations involved FPGA design, embedded programming, and analog RF/Microwave design. In 2013, he joined the Institute National de la Recherche Scientifique, Montreal, Canada, as a Research Assistant in the design and implementation of cognitive radio networks employing software development and FPGA programming. He joined the University of Luxembourg since 2016, where he currently works as a Research Scientist leading the COMMLAB laboratory at the SIGCOM group working on SDR implementation of satellite and terrestrial communication systems.

SHUAI ZHANG (Member, IEEE) received the B.E. degree from the University of Electronic Science and Technology of China, Chengdu, China, in 2007 and the Ph.D. degree in electromagnetic engineering from the Royal Institute of Technology (KTH), Stockholm, Sweden, in 2013. In 2014, he joined Aalborg University, Denmark, where he currently the head of antenna research group with over 12 staff. He has also been admitted to a promotion program to a Professor at Aalborg University since 2022. In 2010 and 2011, he was a Visiting Researcher at Lund University, Sweden and at Sony Mobile Communications AB, Sweden, respectively. He was also an external antenna specialist at Bang & Olufsen, Denmark from 2016-2017. He has supervised/co-supervised 7 Postdocs and 18 PhD students. He has coauthored over 130 articles in well-reputed international journals and over 17 US or WO patents. His citations in Scopus are over 5000 with H index of 38. His current research interests include: millimeter-wave antennas for cellular communications, bio-electromagnetics, metasurfaces, CubeSat antennas, Massive MIMO antennas, wireless sensors, and RFID antennas. He is the Associate Editor for IEEE Antennas and Wireless Propagation Letters; Sensors; and IET Microwaves, Antennas and Propagation. He is also a reviewer for all the top IEEE and IET journals in antenna areas, where he got the prize of "Top Reviewers in IEEE Transactions on Antennas and Propagation 2019-2020 and 2020-2021". He is the General Co-Chair for iWAT2023 at Aalborg, Denmark, the Super Reviewer (previously known as Super TPC or Vice Chair) for IEEE APS 2020 and 2021 and the TPC for several top IEEE conferences. He is the recipient of "IEEE Antennas and Propagation Society Young Professional Ambassador" in 2022, where he gives presentation for different IEEE Chapters on Antennas for Mobile Communications. He has also been intensively invited to international conference and industry to give keynote/plenary speech and presentations. From 2024, he has been the European Association on Antennas and Propagation (EurAAP) Regional Delegate.

PAVEL PECHAC received the M.Sc. and Ph.D. degrees in radio electronics from Czech Technical University in Prague, Czech Republic, in 1993 and 1999, respectively. He is currently the Head of the Department of Electromagnetic Field, Czech Technical University in Prague. His current research interests include radiowave propagation and wireless systems.

VÁCLAV KABOUREK received his master's and doctoral degrees from the Czech Technical University in Prague in 2010 and 2017. His research interests include antenna design and measurement, RCS measurements. His current research activities are also focused on EMC measurements.

SYMEON CHATZINOTAS (Fellow Member, IEEE) received the M.Eng. degree in telecommunications from the Aristotle University of Thessaloniki, Thessaloniki, Greece, in 2003, and the M.Sc. and Ph.D. degrees in electronic engineering from the University of Surrey, Guildford, U.K., in 2006 and 2009, respectively. He is currently a Full-Professor, and the Deputy Head of the SIGCOM Research Group, Interdisciplinary Centre for Security, Reliability, and Trust, University of Luxembourg, Esch-sur-Alzette, Luxembourg, and a Visiting Professor with the University of Parma, Parma, Italy. His research interests include multiuser information theory, cooperative/ cognitive communications, and wireless network optimization. He has been involved in numerous research and development projects with the Institute of Informatics Telecommunications, National Center for Scientific Research Demokritos, Institute of Telematics and Informatics, Center of Research and Technology Hellas, and Mobile Communications Research Group, Center of Communication Systems Research, University of Surrey. He has coauthored more than 400 technical papers in refereed international journals, conferences and scientific books. He was the co-recipient of the 2014 IEEE Distinguished Contributions to Satellite Communications Award, the CROWNCOM 2015 Best Paper Award, and the 2018 EURASIP JWCN Best Paper Award. He is currently on the Editorial Board of the IEEE Open Journal of Vehicular Technology and the International Journal of Satellite Communications and Networking.